Link sito dell'editore:
https://www.sciencedirect.com/science/article/pii/S1270963816308859?via%3Dihub

Link codice DOI: 10.1016/j.ast.2016.10.015

Citazione bibliografica dell'articolo:

Giulio Avanzini, Emanuele L. de Angelis, Fabrizio Giulietti, "Optimal performance and sizing of a battery-powered aircraft", Aerospace Science and Technology, Vol. 59, Dic. 2016, pp. 132-144

Optimal Performance and Sizing of a Battery-Powered Aircraft

Giulio Avanzini[a,1], Emanuele L. de Angelis[*,b,2], Fabrizio Giulietti[b,3]

[a] *University of Salento, Lecce, Italy 73100*
[b] *University of Bologna, Forlì, Italy 47121*

Abstract

This paper presents an analytical and experimental framework for investigating the performance of fixed-wing electrically-driven propeller aircraft. After the experimental derivation of a novel constant power discharge model for lithium-polymer (Li-Po) batteries, closed-form expressions for flight endurance and range are derived by equating power required in steady level flight with power supplied by the battery pack. Best endurance and best range airspeed are obtained. A methodology is also described to optimally size the battery capacity for a given set of battery and aircraft characteristics. The proposed approach is validated by application to a test case relative to a small-size unmanned aerial vehicle.

1. Introduction

The interest in Remotely Piloted Aerial Systems has been steadily and rapidly increasing over the last 15 years, starting from applications in academic research to nowadays widespread operative scenarios in both civil and military applications. In particular, such platforms represent a great potentiality in the field of aerial photography and 3D reconstruction, environmental monitoring [1], disaster prevention and relief [2], and search and rescue operations [3]. According to the particular requirement, different kinds of vehicles and propulsive systems are currently employed. Rotary-wing configurations gained a particular relevance, thanks to their hovering, vertical take-off and landing capabilities, and to the ability of flying in confined spaces. On the other hand, when higher velocity and/or higher altitude and/or longer range are required, fixed-wing aircraft represent the most suitable solution.

*Corresponding author
[1]Professor, Department of Engineering for Innovation (DII), giulio.avanzini@unisalento.it
[2]Research Fellow, Department of Industrial Engineering (DIN), emanuele.deangelis4@unibo.it
[3]Associate Professor, Department of Industrial Engineering (DIN), fabrizio.giulietti@unibo.it

July 28, 2016

Expressions to estimate the endurance and range of piston-propeller and jet aircraft are long-standing results (e.g., Breguet equations), where the aircraft is subject to a decrease of weight caused by fuel consumption [4]. Conversely, the analysis of performance for battery-powered aircraft represents a relatively recent topic of discussion [5, 6]. In steady rectilinear level flight, the battery pack is required to deliver an electrical power which equates the power dissipated by aerodynamic drag, accounting for losses due to the propeller, motor, and motor controller. If the same battery pack also supplies energy to payload and avionic system, a further share of electrical power needs to be considered in the energy balance equation. Note that, if on one side such equation is straightforward, on the other hand modeling of the battery behavior is far from trivial, when effective battery capacity depends on temperature, aging, cycling, and current drawn. The so-called Peukert law suggests a power relationship between discharge current and delivered capacity over some specified range of discharge currents [7]. Peukert equation was empirically proven for lead-acid batteries, but its validity was recently tested for different types of batteries (e.g, lithium-ion batteries), in the case of constant discharge current [8].

In Ref. [9] endurance and range equations are derived using Peukert law for the determination of discharge time as a function of the current drawn, which in turn is obtained from the expression of necessary power. The maximum endurance and the corresponding best endurance condition are evaluated and later validated by means of an experimental investigation [10]. An approximation for maximum range and best range airspeed is also derived, which provides the exact result only in the case of an ideal battery, when Peukert exponent n is equal to 1 and the delivered capacity is thus independent of the discharge current. In Ref. [11] the exact analytical expression for the best range condition is derived for the general case ($n \neq 1$). It is important to underline that the results in [9] and [11] are valid under the hypothesis of constant discharge current and constant battery voltage. The latter is a major simplifying assumption, provided that battery voltage slowly, yet steadily, decreases during the discharge process and higher currents are thus required to provide the same power to the electric motor [12]. On the other hand, a closed-form solution is no longer available when the variation of voltage with battery charge is then taken into account, even in the case of an elementary discharge model like the one proposed in [12] and [13].

For many applications of interest, a constant power discharge process is more representative of the actual battery loading, as it happens for a steady-level flight of a fixed-wing aircraft or a hovering condition of a multi-rotor vehicle. In Ref. [14] an open-circuit voltage discharge model for the constant-power case is proposed, provided battery specifications are known (including internal resistance, Peukert coefficient, etc...). The effect of discharge rate on available capacity is taken into account by modifying Peukert equation for variable current discharges.

In the present paper, a novel integral formulation for constant power battery discharge process is proposed, where time is directly expressed as a function of discharged capacity and absorbed power. The model is based on an extensive

experimental campaign performed on Li-Po batteries, one of the most popular choices for unmanned aerial vehicles, due to the high energy-to-weight ratio, the capability of high-rate discharge, and the variety of shapes and sizes. As an advantage with respect to existing models for constant-power discharge processes, the integral model here proposed does not require the knowledge of voltage variations as a function of current and residual capacity. This in turn allows for a closed-form solution to both the endurance and range equations of electrically-driven propeller aircraft, without the need for simplifying assumptions or numerical discretization required for the use of constant voltage models or models derived from Peukert law. Results are analyzed and compared to the models introduced in [9] and [11]. Some considerations on the effect of ambient temperature on battery performance are also included in the discussion.

Finally, an optimal sizing approach for the battery pack is derived, extending the method proposed in [15] for rotary-wing unmanned aerial vehicles to the case of fixed-wing battery-operated aircraft. Excluding the possibility of extending range and/or endurance by dumping exhausted batteries out of the aircraft in flight [16], and starting from the balance equation of required and available power, a model is derived in [15], where the endurance of a multi-rotor vehicle in hovering condition is expressed as a function of airframe features, rotor figure of merit, payload required power, and on-board battery capacity, based on Peukert discharge model. In such a way, a condition for maximum endurance is determined in terms of optimum capacity and weight, thus allowing to properly size the battery pack with respect to the vehicle take-off weight.

In this paper, a similar approach is derived for the battery sizing of a fixed-wing aircraft for both endurance and range optimization, based on the novel constant-power discharge model. The model is here modified in order to express discharge time as a function of battery nominal capacity. The conditions for battery pack size that provide maximum endurance or maximum range are derived for the most general case, by means of a numerical root-finding procedure. A particular analytical solution is also obtained for maximum endurance, when systems power P_s is neglected or provided by a dedicated battery. These results represent a valuable instrument when aircraft design process is at a conceptual stage.

All the derivations carried out in this paper are applied to a practical case relevant for current technologies, which limit the use of wholly-electrically powered aircraft to the domain of small-size unmanned aerial vehicles. Nonetheless, it is worth highlighting that the principles developed for the determination of best-endurance and best-range conditions, as well as the sizing procedure, are of general validity and, consequently, they could be easily extended to future electrically-driven manned aircraft [17, 18].

In the next section the battery model is presented, based on experimental results conducted by means of a programmable electronic load. In Section 3 the power required for steady level flight is evaluated and endurance and range equations are solved. The best airspeed values are obtained as a function of battery features. In Section 4 the sizing of battery capacity is performed for both endurance and range optimization. Numerical simulations and a laboratory-

test campaign, validating the effectiveness of the proposed approach, are then presented in Section 5. A section of concluding remarks ends this paper.

2. Battery Model

2.1. Experimental Setup

In this Section, a battery discharge model is derived on the basis of experimental results. All tests are performed on Li-Po battery packs at room temperature, $T_0 = 23°\text{C}$, by means of a Maynuo® M9715 DC electronic load, which allows discharge programs at constant voltage, current, load resistance, or power. In particular, each experiment is conducted at constant battery power, defined as

$$P_b = \mathcal{V} I \tag{1}$$

where $\mathcal{V}$ is the voltage across the terminals of the battery when the discharge current I is delivered. Since $\mathcal{V}$ decreases during the discharge process, the experiments are conventionally terminated when the open-loop battery voltage, $\mathcal{V}_{OL}$, reaches the nominal voltage, $\mathcal{V}_0 = N \cdot \mathcal{V}_{cell}$, where $N \in \mathbb{N}_0$ is the number of series-connected cells and $\mathcal{V}_{cell} = 3.7$ V is the nominal open-loop voltage of a single Li-Po cell. In such a way, the battery is prevented to operate in the over-discharging zone and to be damaged. The open-loop voltage can be estimated by means of Ohm's Law, namely

$$\mathcal{V}_{OL} = \mathcal{V} + R\,I \tag{2}$$

where $R\,I$ is the voltage loss caused by battery internal resistance and polarization of the active materials during discharge. The resistance, R, which is largely independent of the state of charge, increases as the battery ages and cycles, and it depends on battery temperature, $T_b = T_0 + \Delta T_{joule}$, where $\Delta T_{joule} = \Delta T_{joule}(I) > 0$ is the temperature increase due to Joule effect and T_0 represents battery temperature at the beginning of each experiment. Different methods are available in the literature to measure R. In this study, a sample test is performed on an aged $N = 6$ cells Li-Po battery manufactured by Robbe®, with a nominal capacity $C_0 = 5$ Ah and a nominal voltage $\mathcal{V}_0 = 6 \cdot 3.7 = 22.2$ V. Internal resistance is evaluated by means of the electronic load according to the current-off method [19], performed at different discharge currents. Results are reported in Fig. 1, where the circle markers represent the values of R obtained experimentally as a function of I. A polynomial regression is proposed in order to fit the experimental data, namely

$$R(I) = \sum_{j=0}^{3} r_j\, I^j \tag{3}$$

where $r_0 = 6.23 \cdot 10^{-2}\,\Omega$, $r_1 = -4.17 \cdot 10^{-4}\,\Omega\,\text{A}^{-1}$, $r_2 = 3.11 \cdot 10^{-6}\,\Omega\,\text{A}^{-2}$, and $r_3 = -1.16 \cdot 10^{-8}\,\Omega\,\text{A}^{-3}$. Internal resistance decreases for higher discharge currents. Since battery temperature T_b increases as a consequence of Joule

effect, internal chemical reactions are accelerated. Battery pack sealing, external surface area, and housing also affect heat transfer to the environment, thus influencing T_b. High temperatures thus improve performance at the cost of increasing unwanted parasitic chemical reactions, resulting in a corresponding loss of battery life [20].

2.2. Constant Power Discharge Model

In the first set of experiments, the battery is discharged at 4 different power levels, namely 50 W, 100 W, 200 W, and 300 W, starting from a fully charged condition. The results are described in Figs. 2 and 3, where the measured closed-loop voltage and current are plotted as a function of the discharged capacity, C, obtained as

$$C(t) = \int_0^t I(s)\, ds \tag{4}$$

and reported in terms of Depth of Discharge (DOD), which represents the percentage of discharged capacity with respect to the nominal capacity, C_0. Battery voltage decreases during the discharge process, and higher currents become necessary to provide the same power required by the electrical load. Hence, for a given time t, discharged capacity increases with the requested power (see Fig. 4, where discharge time is reported as a function of discharged capacity). Taking into account the results reported in Fig. 4, a battery model is presented where time, t, is a function of discharged capacity, C, and requested power, P_b. Assume

$$t(C, P_b) = \alpha\, C^{\beta'} \tag{5}$$

where α and β' are positive functions of power and battery parameters (for example, the number of cells, N), to be identified experimentally.

In order to characterize the model proposed in Eq. (5) for different battery configurations, a second set of experiments is considered. Different Li-Po battery packs are tested with $N = 1, 2, 4, 6$ cells, each one produced by a different manufacturer (Nano-Tech®, FightPower®, Turnigy®, Robbe®, respectively). For each pack, 4 different power levels are set, for a total of 16 experiments. Note that each battery pack was previously characterized in terms of internal resistance at room temperature, in order to stop the experiments when $\mathcal{V}_{OL} \equiv \mathcal{V}_0$, disregarding the characteristics of discharge process used for the particular test. After each constant-power discharge test, a least squares algorithm is used for evaluating the coefficients α and β' that best fit the model proposed in Eq. (5) to the experimental data points. In Table 1 the experimental results are reported, with the desired power, P_b, set on the electronic load, the mean value, $\overline{P}_b$, of the actual power discharged, and the values of α and β' resulting from the selected nonlinear curve-fitting algorithm. Note that α shows to be a decreasing function of power, $\overline{P}_b$, and approximately proportional to N. On the other hand, no trend is identifiable for β', and a constant value equal to the mean value, $\beta = 0.9664$, calculated from Table 1, can be assumed for the model in Eq. (5). A least squares algorithm is used to seek the updated values of α that best fit the the model in Eq. (5), when $\beta' = \beta$. The new values of α

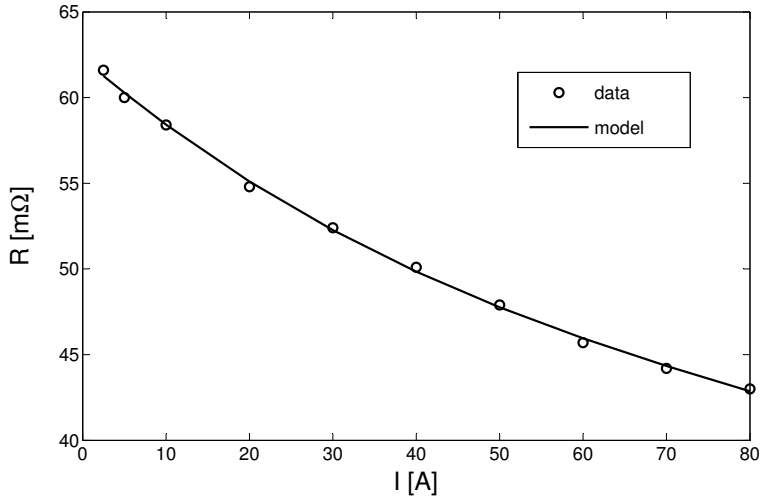

Figure 1: Battery internal resistance ($N = 6$, $T_0 = 23°\mathrm{C}$).

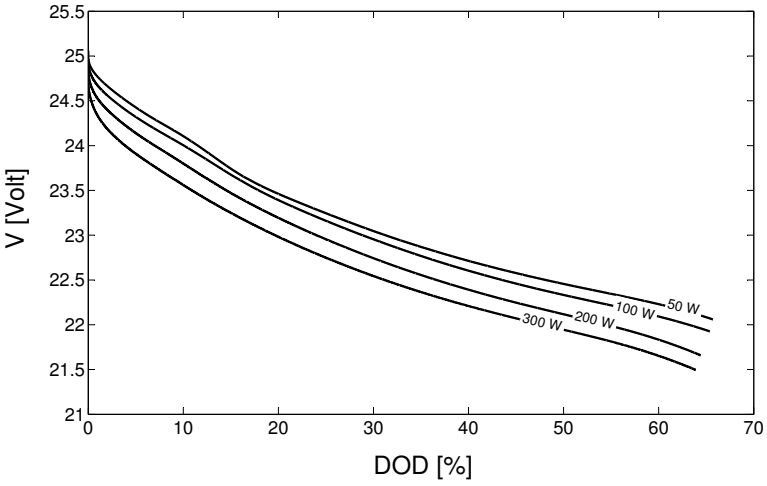

Figure 2: Battery voltage during constant power discharges ($N = 6$, $T_0 = 23°\mathrm{C}$).

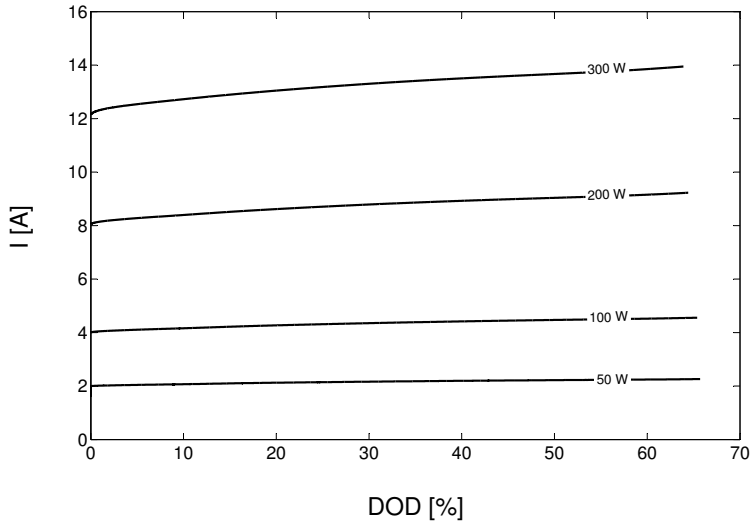

Figure 3: Battery current during constant power discharges ($N = 6$, $T_0 = 23°\mathrm{C}$).

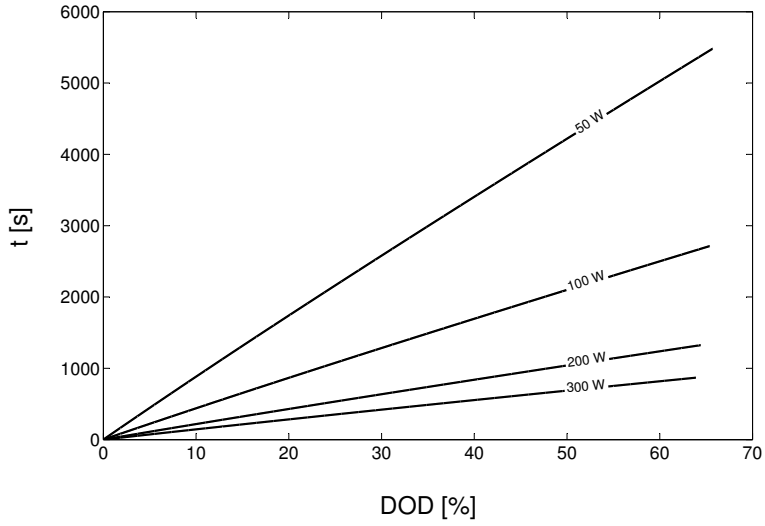

Figure 4: Discharge time during constant power discharges ($N = 6$, $T_0 = 23°\mathrm{C}$).

Table 1: Experimental results (Eq. (5) characterization, $T_0 = 23°C$).

N	$\mathcal{V}_0$ [V]	C_0 [Ah]	P_b	($\overline{P}_b$, $RMSE$) [W]	α	β'	α ($\beta' = \beta$)	$RMSE$ [h]
1	3.7	0.75	2.5	(2.475, 0.002)	1.5045	0.9627	1.5080	0.0025
			5	(4.980, 0.001)	0.7348	0.9613	0.7377	0.0007
			10	(9.977, 0.003)	0.3521	0.9578	0.3545	0.0005
			15	(14.979, 0.004)	0.2221	0.9562	0.2241	0.0003
2	7.4	2.5	10	(9.958, 0.003)	0.7782	0.9670	0.7782	0.0012
			20	(19.952, 0.006)	0.3815	0.9650	0.3814	0.0007
			40	(39.959, 0.008)	0.1830	0.9665	0.1830	0.0003
			60	(59.954, 0.009)	0.1184	0.9769	0.1186	0.0004
4	14.8	5.4	50	(49.904, 0.008)	0.3205	0.9670	0.3206	0.0012
			100	(99.891, 0.011)	0.1581	0.9664	0.1581	0.0006
			200	(199.904, 0.041)	0.0762	0.9828	0.0757	0.0002
			300	(299.932, 0.046)	0.0496	0.9717	0.0498	0.0002
6	22.2	5	50	(49.853, 0.055)	0.4836	0.9659	0.4834	0.0016
			100	(99.855, 0.011)	0.2404	0.9662	0.2404	0.0008
			200	(199.850, 0.026)	0.1193	0.9640	0.1190	0.0005
			300	(299.864, 0.062)	0.0787	0.9656	0.0787	0.0003

are reported in Table 1 with the indication of the algorithm Root Mean Square Error (RMSE).

A test-retest procedure is also performed in order to evaluate the measurement repeatability under the same experimental conditions. In particular, for each battery pack and each constant-power value, the test-retest variability of α proves to be very small over four equal experiments, provided $\beta' = \beta$. The case represented by the discharge at $P_b = 200$ W of the pack with $N = 6$, for example, shows a dispersion of the obtained α values with $RMSE = 0.0003$ about the reference value reported in Table 1, namely $\alpha = 0.119$.

For each number of series-connected cells, $\alpha(P_b, N)$ is plotted in Fig. 5 as a function of $\overline{P}_b$. For each battery type, α decreases exponentially with $\overline{P}_b$ (see the circle markers). A curve-fitting is thus performed in order to characterize the model

$$\alpha(P_b, N) = \delta(N)\, P_b^{\epsilon(N)} \tag{6}$$

in terms of two coefficients, $\delta(N) > 0$ and $\epsilon(N) < 0$, reported in Table 2, and used to plot the curves in Fig. 5 (see the solid lines). In Fig. 6 the coefficients

Table 2: Experimental results (Eq. (6) characterization, $\beta' = \beta = 0.9664$, $T_0 = 23°C$).

N	$\mathcal{V}_0$ [V]	$\delta(N)$	$\epsilon(N)$
1	3.7	3.872	-1.039
2	7.4	8.471	-1.038
4	14.8	18.18	-1.032
6	22.2	24.96	-1.009

δ and ϵ are plotted as a function of cells number, N (see the circle markers). In

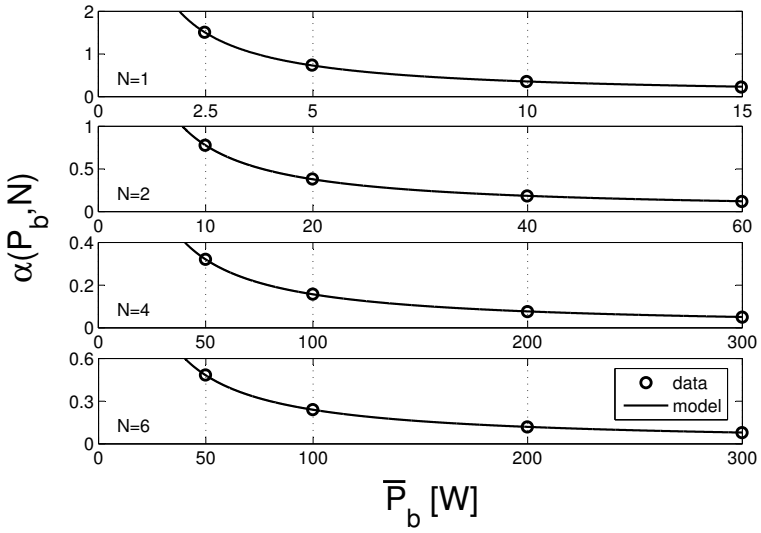

Figure 5: Experimental results (Eq. (6) characterization, $\beta' = \beta = 0.9664$, $T_0 = 23°\mathrm{C}$).

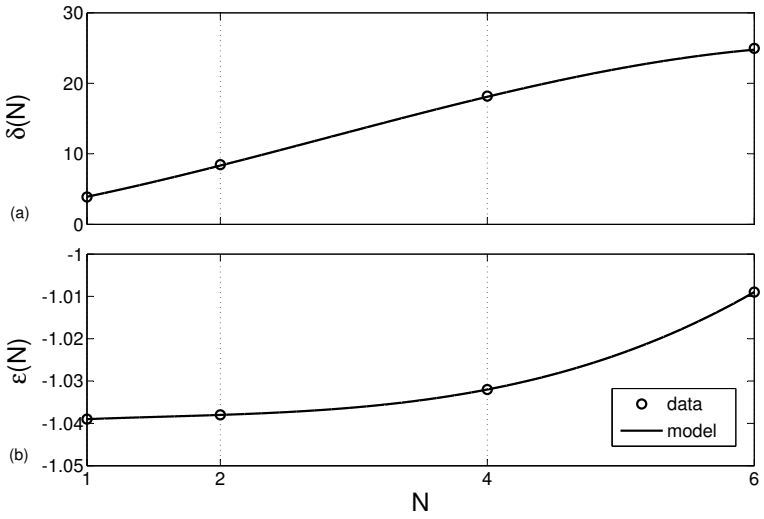

Figure 6: Experimental results (α_0, α_P - characterization, $\beta' = \beta = 0.9664$, $T_0 = 23°\mathrm{C}$).

order to characterize battery configurations other than the ones given in Table 2, the following models are used to identify the functions $\delta = \delta(N)$ and $\epsilon = \epsilon(N)$ for a generic value $N \in \mathbb{N}_0$ (see the solid lines in Fig. 6):

$$\delta(N) = -0.1067\,N^3 + 0.8960\,N^2 + 2.488\,N + 0.6299 \tag{7}$$

$$\epsilon(N) = 2.917 \cdot 10^{-4}\,N^3 - 1.375 \cdot 10^{-3}\,N^2 + 3.083 \cdot 10^{-3}\,N - 1.041 \tag{8}$$

2.3. Temperature Effects and Other Considerations on Battery Performance

As for any empirically derived model, based on experimental results and interpolation techniques, the values of model parameters are related to the particular class of investigated battery and operating conditions (such as battery age, number of discharge/recharge cycles, temperature, etc.). As an example, temperature at which a battery is discharged affects its service life and voltage characteristics, due to the reduction in chemical activity and the increase in the internal resistance of the battery at lower temperatures [20]. In particular, at lower ambient temperature, T_0, and the same discharge power, P_b, a reduction of usable capacity is expected, as well as an increase in the slope of the discharge curve (see [21] for the effect of ambient temperature on valve-regulated lead-acid batteries). In what follows it is investigated how the effects described above of temperature on battery performance influence the coefficients of the model in Eq. (5).

Consider the battery pack tested in Section 2.2, with N=2. A set of constant power discharges is performed with the same power levels (10 W, 20 W, 40 W, and 60 W) at a constant room temperature $T_0 = 17°$C. In particular, each test is stopped at the same value of the closed-loop voltage which was reached at the end of the corresponding test performed at higher temperature. In Fig. 7 a comparison is reported for the 60 W discharge test between the closed-loop voltage time histories. The detrimental effect of lower temperature can be quantified at a given value of discharged capacity. Assuming $C = 1.41$ Ah, the experiment conducted at $P_b = 60$ W shows a decrease of discharge time of the colder battery about 1.92% with respect to the same experiment performed at 23°C. For the sake of brevity, the experimental results are not discussed in detail. The procedure used to estimate the coefficients α and β' that best fit the model in Eq. (5) to the experimental data points provides a mean value to β' given by $\beta = 0.9728$, calculated over four experiments at $T_0 = 17°$C. At this value of β, the curve-fitting technique that allows to characterize the model in Eq. (6) gives $\delta = 8.709$ and $\epsilon = -1.053$ (respectively 2.8% bigger and 1.5% smaller than the corresponding values reported in Table 2 for the case when $T_0 = 23°$C), whose variation denotes the expected decrease of endurance performance.

In general, the parameters that define the variation of δ and ϵ as a function of the number of cells N depend on battery condition and type. For this reason, the experiments were performed on battery packs with exactly the same technology, at approximately half of their operational lifespan, as a compromise between better performance, when the battery pack is new, and degraded conditions, when close to the end of their use. An accurate estimate of discharge time

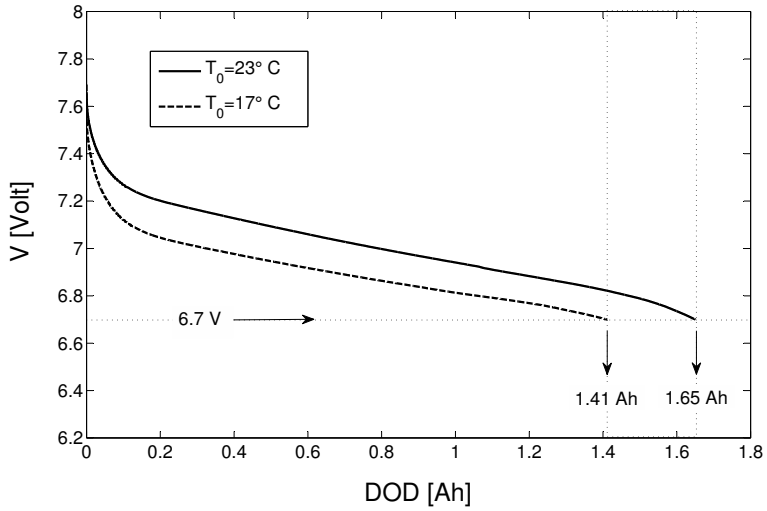

Figure 7: Battery voltage during constant power discharges ($N = 2$, $P_b = 60$ W, different room temperatures).

would thus require to repeat the whole experimental campaign at various stages of battery life. Anyway, to the authors' experience with Li-Po batteries, the trends of $\delta(N)$ and $\epsilon(N)$ are correctly evaluated, with only minor variations. For larger battery packs an ad hoc experimental campaign is also required, to extend the model based on larger values of cells ($N > 6$).

3. Performance Optimization

3.1. Required and Available Power for Cruise Flight

The total power required by an electric aircraft in steady-level flight is

$$P_{tot} = P_s + P_r \tag{9}$$

where $P_s = P_a + P_p$ is the total power required for avionics and possible payload, and P_r is the power required to overcome drag D at a given flight velocity V, namely

$$P_r = DV \tag{10}$$

A parabolic drag polar in the form $C_D = C_{D_0} + kC_L^2$ is assumed, where C_{D_0} is the zero-lift drag coefficient and kC_L^2 is the term related to the induced drag. Remembering that $C_L = 2W/\left(\rho S V^2\right)$, where ρ is air density, S is wing reference area, and W is aircraft weight [9], the power required for cruise flight in Eq. (10) can be written in the form

$$P_r = DV = 0.5\rho V^3 S C_D = AV^3 + BV^{-1} \tag{11}$$

where

$$A = 0.5\rho S C_{D_0}; \quad B = \frac{2kW^2}{\rho S}. \tag{12}$$

In a condition of steady flight, the power required to overcome drag, P_r, and the available power, $P_a = T\,V$, related to the thrust, T, generated by aircraft propeller, are equal. Note however that the power output of the battery dedicated to the propulsion system is reduced by losses within the electric driving system made of a speed regulator, an electric motor, and a propeller. Although each element has its own efficiency, η_r, η_m, and η_p, respectively, for the purpose of the present work, they will be combined into an overall efficiency, $\eta_{tot} = \eta_r\,\eta_m\,\eta_p$, such that

$$\eta_{tot}(P_b - P_s) = P_r \tag{13}$$

where η_{tot} is assumed to be a constant. Taking into account Eqs. (11), (12), and (13), the total power requested from the battery for cruise flight becomes

$$P_b = \bar{A}V^3 + \bar{B}V^{-1} + P_s \tag{14}$$

where

$$\bar{A} = \frac{0.5\rho S C_{D_0}}{\eta_{tot}}; \quad \bar{B} = \frac{2kW^2}{\rho S \eta_{tot}} \tag{15}$$

3.2. Endurance Optimization

For a given usable capacity, battery technology, and ambient temperature, cruise endurance is estimated by means of Eqs. (5) and (6), provided the discharge power is given by Eq. (14). It follows that

$$t = \delta\,P_b^{\epsilon}\,C^{\beta} = \delta\,\left(\bar{A}V^3 + \bar{B}V^{-1} + P_s\right)^{\epsilon}\,C^{\beta} \tag{16}$$

where battery power is assumed to be nonzero. Since $\epsilon \leq -1$, according to the proposed discharge model, one obtains that the best endurance is achieved by flying at minimum-power condition, which occurs at the airspeed [9]

$$V_{be} = \frac{1}{\sqrt[4]{3}}\sqrt[4]{\frac{\bar{B}}{\bar{A}}} \tag{17}$$

Let $E = L/D$ be the aircraft aerodynamic efficiency in the selected cruise condition. A non-dimensional speed ratio $b = V/V_{E_{max}}$ is adopted as in [11], for representing the actual cruise condition with respect to the maximum efficiency condition, $E = E_{max}$, where $V = V_{E_{max}}$. It is easy to express the lift coefficient and the aerodynamic efficiency as a function of b in the form [11]

$$C_L = \frac{1}{b^2}C_{L_{E_{max}}}; \quad E = \frac{2b^2}{1+b^4}E_{max} \tag{18}$$

where both the values of $C_{L_{E_{max}}} = \sqrt{C_{D_0}/k}$ and $E_{max} = 1/\sqrt{4C_{D_0}k}$ depend on the coefficients of the drag polar only and may be thus assumed as fixed, for a given vehicle aerodynamic configuration. Note, in particular, that $V_{Emax} =$

$\sqrt[4]{\bar{B}/\bar{A}}$, such that Eq. (17) provides the optimal value of the airspeed ratio for endurance optimization:

$$b_{be} = 1/\sqrt[4]{3} \tag{19}$$

Note that for higher value of P_s, the endurance is reduced (a greater share of battery power is exploited by on-board systems and payload), but the best endurance flight velocity is unaffected by P_s, being always equal to the minimum-power airspeed.

3.3. Range Optimization

The range of an electrically-driven propeller aircraft is obtained by multiplying the endurance t in Eq. (16) by the airspeed V, namely

$$x = t\,V = \delta\,V\,P_b^{\epsilon}\,C^{\beta} = \delta\,V\,\left(\bar{A}V^3 + \bar{B}V^{-1} + P_s\right)^{\epsilon}\,C^{\beta} \tag{20}$$

Note that, according to the battery model coefficients obtained in Section 2, the endurance in Eq. (16) is expressed in hours, h. Hence, a conversion factor equal to 3.6 should be taken into account if a range expressed in kilometers is desired.

The optimal value for the best range airspeed is obtained by equating to zero the derivative of range x with respect to V in Eq. (20), namely

$$\begin{aligned}\frac{dx}{dV} = \delta\,V^{-\epsilon}\,&\left[\bar{A}\,(1+3\epsilon)\,V^4 + P_s\,V + \bar{B}\,(1-\epsilon)\right]\\ &\times\left(\bar{A}V^4 + P_s\,V + \bar{B}\right)^{\epsilon-1}\,C^{\beta} = 0\end{aligned}$$

This yields the condition

$$\bar{A}\,(1+3\epsilon)\,V^4 + P_s\,V + \bar{B}\,(1-\epsilon) = 0 \tag{21}$$

that can be analytically solved.

In the case when the power absorbed by aircraft avionics and payload is negligible ($P_s \approx 0$ W), Eq. (21) gives

$$V_{br}^{\star} = \sqrt[4]{\frac{\epsilon-1}{1+3\epsilon}}\,\sqrt[4]{\frac{\bar{B}}{\bar{A}}} \tag{22}$$

and the best airspeed ratio is

$$b_{br}^{\star} = \sqrt[4]{\frac{\epsilon-1}{1+3\epsilon}} \tag{23}$$

Note also that, if $\epsilon = -1$, the ideal situation in which discharge time is simply inversely proportional to the absorbed power is obtained. In such a particular case, the ideal best range condition identified in [9] for ideal discharge process with unity Peukert coefficient, $n = 1$, is recovered by Eqs. (22) and (23), which give $V_{br}^{\star} \equiv V_{E_{max}}$ and $b_{br}^{\star} \equiv 1$, respectively.

Consider now the general case represented by Eq. (21). Let

$$\Delta_0 = 12\,\bar{A}\bar{B}\,(1+3\epsilon)\,(1-\epsilon)\,; \quad \Delta_1 = 27\,\bar{A}P_s^2\,(1+3\epsilon) \tag{24}$$

and

$$Q = \sqrt[3]{\frac{\Delta_1 + \sqrt{\Delta_1^2 - 4\,\Delta_0^3}}{2}}; \quad R = \frac{1}{2}\sqrt{\frac{1}{3\,\bar{A}\,(1+3\epsilon)}\left(Q + \frac{\Delta_0}{Q}\right)} \tag{25}$$

Provided $\epsilon \leq -1$, it is possible to prove that the fourth order polynomial in Eq. (21) always has one pair of complex conjugate roots. One of the remaining real solutions is always negative. The only real positive solution provides the value of the best range airspeed in the form [22]

$$V_{br} = R + \frac{1}{2}\sqrt{-4R^2 - \frac{P_s}{R\,\bar{A}\,(1+3\epsilon)}} \tag{26}$$

and the best airspeed ratio

$$b_{br} = \sqrt[4]{\frac{\bar{A}}{\bar{B}}}\left[R + \frac{1}{2}\sqrt{-4R^2 - \frac{P_s}{R\,\bar{A}\,(1+3\epsilon)}}\right] \tag{27}$$

for range optimization. For higher values of P_s, the range obtained from Eq. (20) for $V = V_{br}$ derived in Eq. (26) steadily decreases, whereas the best range airspeed increases, as it will be shown numerically in Section 5.

4. Sizing of Battery Capacity

4.1. Preliminary Considerations

In Section 3 the best endurance and best range conditions were determined on the basis of the proposed battery discharge model in terms of airspeed in steady level flight for a given aircraft configuration (total weight, geometric and aerodynamic characteristics, battery size, etc.). Contrary to what happens in conventional fuel-powered aircraft, for which weight steadily decreases during cruise and an increased fuel fraction always provides increased endurance and range, the weight of electrically-powered aircraft remains constant and the beneficial effect of weight loss during cruise is not experienced, as qualitatively highlighted in the introduction. As a consequence, increasing battery weight may not necessarily provide an increased endurance and/or range, if the energy cost of lifting more weight during the whole cruise overcomes the benefit of the increased battery-pack capacity.

In this section, the optimal value of the battery pack that maximizes either endurance or range is determined, following an approach similar to that described in [15], where the optimal battery pack sizing was obtained for a multirotor configuration using the classical Peukert discharge model. In the present case, the novel battery discharge model is applied to the case of fixed-wing electric aircraft, in order to derive useful guidelines for sizing the battery pack during the conceptual design phase for this class of vehicles.

First of all, it is necessary to rearrange the expression of the electrical power, P_b, as a function of aircraft weight. From Eqs. (11) and (13) it is $P_b = DV/\eta_{tot} +$

P_s. Taking into account the definition of aerodynamic efficiency, E, and the parametrization introduced in Eq. (18), the power requested from the battery can be expressed as an explicit function of total aircraft weight, namely

$$P_b = \frac{WV}{E\,\eta_{tot}} + P_s = \nu(\rho)\,\mu(b)\,W^{3/2} + P_s \tag{28}$$

where

$$\mu(b) = \frac{1+b^4}{2b\,E_{max}\,\eta_{tot}} \tag{29}$$

is a function of the selected airspeed condition and

$$\nu(\rho) = \sqrt{\frac{2}{\rho S C_{L_{E_{max}}}}} \tag{30}$$

depends on cruise altitude.

Aircraft weight, which explicitly appears in Eq. (28), can be conveniently decomposed into

$$W = W_{eo} + W_p + W_b \tag{31}$$

where W_{eo} is the operative empty weight (that includes structure, propulsion system, and avionics weight), W_p is payload weight, and W_b is battery weight. At a conceptual design stage, it is possible to express the operative empty weight fraction as a function of takeoff weight, in the form

$$(W_{eo}/W) = \Gamma W^{\gamma} \tag{32}$$

where the regression coefficients Γ and γ are obtained from statistics based on available data for the considered class of aircraft [23]. In the present application, data from [24] are used for the determination of values for Γ and γ, valid for electrically-powered remotely piloted vehicles.

As discussed in [25], it is possible to assume that wing surface S scales approximately as $W^{2/3}$. Thus, assuming S_{ref} and W_{ref} as wing surface and takeoff weight of a reference aircraft, respectively, one gets

$$S = S_{ref}(W/W_{ref})^{2/3} \tag{33}$$

In order to allow for quantitative comparison, the aircraft model considered in [9] will be taken as a reference for the study in the numerical example proposed in the next section. Equation (28) thus achieves the form

$$P_b = \psi(b,\rho)\,W^{7/6} + P_s \tag{34}$$

where $\psi(b,\rho) = \mu(b)\,\nu_{ref}(\rho)W_{ref}^{1/3}$ and $\nu_{ref}(\rho)$ is obtained from Eq. (30) for $S = S_{ref}$.

Finally, let $\sigma = W_b/E_0 = W_b/\left(\mathcal{V}_0\,C_0\right)$ indicate battery weight/energy ratio (that is, the inverse of battery energy density). Hence, aircraft total weight in Eq. (31) can be rewritten as

$$W = W_p + (W_{eo}/W)W + W_b = W_p + \Gamma W^{\gamma+1} + \sigma\mathcal{V}_0\,C_0 \tag{35}$$

In what follows, aircraft sizing will be performed assuming takeoff weight W as the independent variable and determining battery capacity from Eq. (35),

$$C_0 = \frac{W - W_p - \Gamma W^{\gamma+1}}{\sigma \mathcal{V}_0} \tag{36}$$

4.2. Battery Sizing for Endurance Optimization

Consider Eq. (16) and the expressions of battery power and nominal capacity respectively given by Eqs. (34) and (36). Assume, without loss of generality, that the nominal capacity C_0 is fully discharged during the cruise and that the airspeed ratio b is equal to the optimal value in Eq. (19), $b_{be} = 1/\sqrt[4]{3}$. Hence

$$t = \delta \left(\psi_{be}\, W^{7/6} + P_s\right)^{\epsilon} \left(\frac{W - W_p - \Gamma W^{\gamma+1}}{\sigma \mathcal{V}_0}\right)^{\beta} \tag{37}$$

where $\psi_{be} = \psi(b_{be}, \rho)$. The battery configuration for maximum endurance is obtained by taking the derivative of t with respect to W and imposing $dt/dW = 0$. This leads to the equation

$$\begin{aligned} f_t(W) = {} & 7\epsilon\psi_{be}\, W^{1/6} \left(W - W_p - \Gamma W^{\gamma+1}\right) \\ & - 6\beta \left[(\gamma+1)\Gamma W^{\gamma} - 1\right] \left(\psi_{be}\, W^{7/6} + P_s\right) = 0 \end{aligned} \tag{38}$$

To the best of the authors' knowledge, Eq. (38) cannot be solved analytically in the most general case. Hence, a numerical method is required (e.g. Newton's iterative scheme [26]) in order to obtain a solution for the optimal weight W_{be} and the corresponding C_{0be}. An analytical solution to Eq. (38) can be obtained when no payload is required to be carried on board, such that $W_p = 0$ N and $P_p = 0$ W. Assuming the power required for aircraft avionics is negligible ($P_a \approx 0$ W), one gets

$$W^{\star}_{be} = \left[\frac{(6\beta + 7\epsilon)\,/\,\Gamma}{6\beta\,(\gamma+1) + 7\epsilon}\right]^{1/\gamma} \tag{39}$$

while the corresponding battery capacity is given by Eq. (36) for $W = W^{\star}_{be}$.

4.3. Battery Sizing for Range Optimization

The optimal aircraft configuration which maximizes range for a given payload achieves the best performance by flying at the best range airspeed identified by Eq. (27). From the definitions in Eqs. (15), (24), and (25), it is evident that the best range airspeed ratio b_{br} depends on aircraft weight W and is influenced by battery parameters and power required by the payload. For the sake of clarity, the functional argument of b_{br} will be omitted in what follows.

Aircraft range is obtained by multiplying endurance in Eq. (37) times the airspeed $V_{br} = b_{br}\, V_{Emax}$, where V_{Emax} can be written as

$$V_{Emax} = \nu(\rho)\, W^{1/2} = \psi_{br} \mu_{br}^{-1}\, W^{1/6} \tag{40}$$

according to Eqs. (30) and (35), provided $\psi_{br} = \psi(b_{br}, \rho)$, $\mu_{br} = \mu(b_{br})$, and $b_{br} = b_{br}(W)$. Hence, since $x = t\,V$, it is

$$x = b_{br}\,\delta\left(\psi_{br}\mu_{br}^{-1}\,W^{1/6}\right)\left(\psi_{br}\,W^{7/6} + P_s\right)^{\epsilon} \times \left(\frac{W - W_p - \Gamma W^{\gamma+1}}{\sigma\mathcal{V}_0}\right)^{\beta} \tag{41}$$

The size of the battery pack that maximizes range performance should be obtained by taking the derivative of x with respect to W and solving the equation $dx/dW = 0$. Unfortunately, the complexity of the expression of the derivative precludes, to the best of the authors' knowledge, the possibility of an analytical solution. As a consequence, the function that relates aircraft total weight to the expected range performance in Eq. (41) is plotted and the best range configuration is identified either graphically on the plot or numerically, by means of a simple root-finding algorithm, such as the parabolic search or the simplex method [27, 28].

5. Numerical Example

5.1. Performance Optimization

In what follows, the battery model derived in Section 2 and the approach presented in Sections 3 and 4 for endurance and range performance optimization and battery sizing of an electrically-driven propeller aircraft are validated by means of numerical simulations and an experimental campaign. The small-size electrical aircraft used as an example in [9], taken from [29], is considered (see Table 3), with a Li-Po battery pack characterized by $N = 3$, $\mathcal{V}_0 = 11.1$ V, and $C_0 = 2.2$ Ah (battery type not tested in Section 2 for model identification). Taking into account Eqs. (7) and (8), the battery-model coefficients are $\delta = 13.28$ and $\epsilon = -1.036$. Provided $S = S_{ref} = 0.32$ m^2 and $W = W_{ref} = 9.34$ N, one has $\bar{A} = 5.760{\cdot}10^{-3}$ kg m^{-1} and $\bar{B} = 1.181{\cdot}10^{2}$ kg m^3 s^{-4} from Eq. (15). Let $P_s = 5$ W be the power required for avionics and payload. Provided $V_{Emax} = \sqrt[4]{\bar{B}/\bar{A}} \approx 12$ m s^{-1} at the maximum aerodynamic efficiency $E_{max} = 11.32$, the total power required to the battery for cruise flight is plotted in Fig. 8 as a function of the airspeed ratio, b [see Eq. (14)].

Flight endurance expressed in minutes as given by Eq. (16) is reported in Fig. 8 for different values of discharged capacity. Note that the best endurance condition is exactly located by Eq. (19), where $b = b_{be} = 1/\sqrt[4]{3}$ and $P_b = P_{bmin} = 22.32$ W (see Table 4). An experiment is also performed where a FullPower® battery pack with the above characteristics is discharged by means of the electrical load to the 80% of the nominal capacity C_0 at the constant power $P_b = P_{bmin} = 22.32$ W. In such a case, the discharge time is equal to $t_{exp} = 54.6$ min (see the circle marker in Fig. 8). In order to validate the proposed battery model, the same values of discharged capacity and power are respectively substituted in Eq. (16), to obtain $t_{mod} = 55.1$ min, with an estimation error about 0.86%.

Table 3: Reference aircraft and battery data.

Parameter	Symbol	Value	Units
Aircraft			
Drag polar coefficients	C_{D0}	0.015	
	k	0.13	
Total efficiency	η_{tot}	0.5	
Air density	ρ	1.2	$\mathrm{kg\,m^{-3}}$
Wing area	S_{ref}	0.32	$\mathrm{m^2}$
Weight	W_{ref}	9.34	N
Battery pack			
Peukert coefficient	n	1.107	
No. of cells	N	3	
Nominal voltage	$\mathcal{V}_0$	11.1	V
Nominal capacity	C_0	2.2	Ah
System power	P_s	5	W

As a final consideration, the validity of the proposed battery model is compared to a classical Peukert-based approach, where the assumption of constant current during battery discharge is considered, as indicated in Eq. (9) from [9]. In the present framework, an equivalent constant voltage is considered as the mean value between the open-loop fully charged battery voltage and the nominal voltage, namely $\mathcal{V}_e = (\mathcal{V}_f + \mathcal{V}_0)/2 = 11.85$ V, provided $\mathcal{V}_f = 12.6$ V. It follows that the equivalent constant current relative to a discharge at $P_b = P_{bmin} = 22.32$ W is $I_{pk} = P_{bmin}/\mathcal{V}_e = 1.88$ A. Let R_t be the battery hour rating, that is the discharge time over which the nominal capacity was determined by the manufacturer (typically 1 h for small rechargeable battery packs). Provided $n = 1.107$ is the Peukert coefficient estimated for the considered battery, predicted endurance is $t_{pk} = R_t^{1-n}\left(0.8 \cdot \mathcal{V}_e\, C_0/P_{bmin}\right)^n \cdot 60 = 55.7$ min (see the square marker in Fig. 8), with an estimation error about 2%. As a final consideration, note that both Peukert approach and the proposed method provide the same best endurance airspeed ratio.

The procedure outlined above is also followed for range characterization. Flight range as given by Eq. (20) is reported in Fig. 9 for different values of discharged capacity. The best range condition is evaluated by Eqs. (24)-(27), providing $V_{br} = 12.6\ \mathrm{m\,s^{-1}}$ and $b = b_{br} = 1.051$ at the constant power value $P_b = 25.84$ W. The considered battery pack with $N = 3$ cells is discharged by means of the electrical load to the 80% of nominal capacity C_0 at the constant power $P_b = 25.84$ W. In such a case, the discharge time results to be $t_{exp} = 47.7$ min, corresponding to a range $x_{exp} = 36.08$ km (see the circle marker in Fig. 9). In order to validate the proposed battery model, the same values of discharged capacity and power are substituted in Eq. (20), to obtain $t_{mod} = 47.3$ min and $x_{mod} = 35.69$ km, with an estimation error about 1.08%.

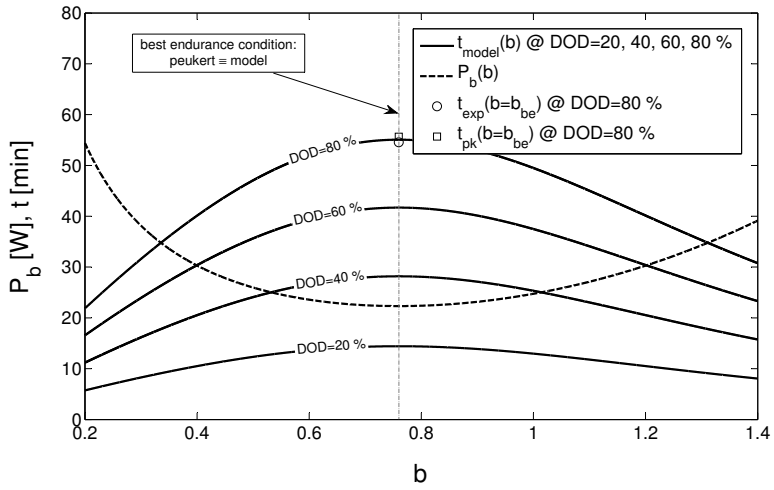

Figure 8: Endurance (—) and power (- - -) as a function of airspeed ratio ($N = 3$).

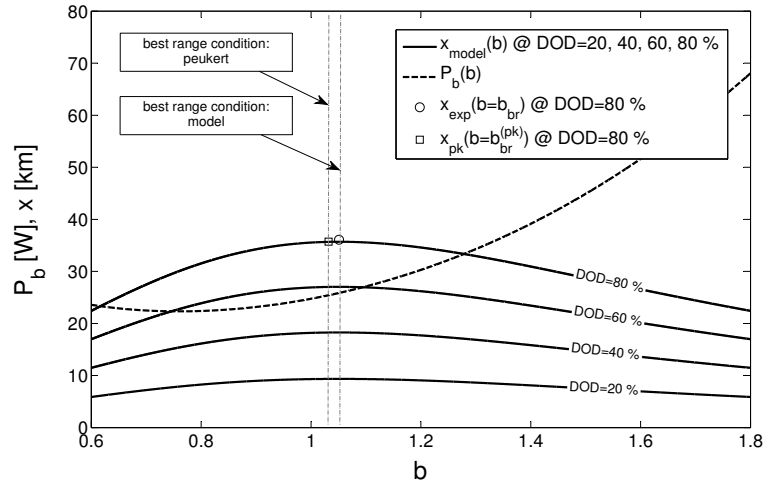

Figure 9: Range (—) and power (- - -) as a function of airspeed ratio ($N = 3$).

With regard to the range equation, a comparison is also provided between the proposed model and a Peukert-based approach [see Eq. 5 from [11]]. Taking into account the contribution of $P_s = 5$ W (not considered in [11]), it is straightforward to prove that the best range condition results into $b = b_{br}^{(pk)} = 1.032$, where $P_b = 25.41$ W, the equivalent current is $I_{pk} = P_b/\mathcal{V}_e = 2.14$ A, and $x_{pk} = R_t^{1-n}\,(0.8 \cdot \mathcal{V}_e\, C_0/25.41)^n \cdot b_{br}^{(pk)} V_{Emax} \cdot 3.6 = 35.72$ km (see the square marker in Fig. 9). The estimation error between x_{pk} and x_{exp} is about 1%.

Table 4: Experimental validation of results for optimal performance.

Discharge model	Endurance: t_{be} [min]			Range: x_{br} [km]		
	b_{be}	$P_b(b_{be})$ [W]	theory (exp.)	b_{br}	$P_b(b_{br})$ [W]	theory (exp.)
Proposed model	$1/\sqrt[4]{3}$	22.32	55.1 (54.6)	1.051	25.84	35.69 (36.08)
Peukert model	$1/\sqrt[4]{3}$	22.32	55.7 (54.6)	1.032	25.41	35.72 (-)

5.2. Battery Sizing

In what follows, the battery-sizing problem analyzed in Section 4 is investigated by scaling the fixed-wing platform considered above, mounting a Li-Po battery with a weight-energy ratio $\sigma = 0.0763$ N $(\text{Wh})^{-1}$. The regression coefficients introduced in Eq. (32) are obtained from the data reported in the UAS database in Appendix C of [24]. The resulting coefficients are given by $\Gamma = 0.6998$ and $\gamma = -0.0890$. It is assumed that $P_a = 1$ W and a 80% usage of nominal capacity C_0 is considered. Provided $C_{L_{Emax}} = 0.34$, from Eq. (30) it is $\nu_{ref}(\rho) = 3.92$ $\text{kg}^{-1/2}$ $\text{m}^{1/2}$. The non-dimensional parameter defined by Eq. (29) is $\mu(b_{be}) = 0.16$ and the coefficient in Eq. (34) is $\psi(b_{be}, \rho) = 1.28$. The payload is represented by an infrared camera designed for miniature unmanned aerial vehicles, here named Camera 1 ($W_p = 0.186$ kgf, $P_p = 2.5$ W). A lighter and smaller version of the same device, here named Camera 2 ($W_p = 0.114$ kgf, $P_p = 1.5$ W), is also considered in order to provide further insight into the sizing process under different payload requirements [30].

Figure 10.a shows the variation of maximum flight endurance as determined from Eq. (37) as a function of aircraft weight for two different payload configurations and three battery packs characterized by the same technology and $N = 2$, 3, and 4 cells connected in series, respectively. The function $f_t(W)$ in Eq. (38), which is proportional to the derivative of the endurance dt/dW in Eq. (37), is plotted as a function of aircraft weight for $N = 3$ and both payloads in Fig. 10.b, highlighting that best endurance configurations are obtained when Eq. (38) is satisfied. Best endurance configurations for all the payloads and cell number are listed in Table 5, together with battery parameters obtained from Eqs. (7) and (8). The presence of a maximum in all the curves clearly points out that, if endurance is pursued as the most relevant goal in the design process, it is useless to increase the size of the battery pack beyond a certain limit, provided that the corresponding growth in aircraft weight affects necessary power for the

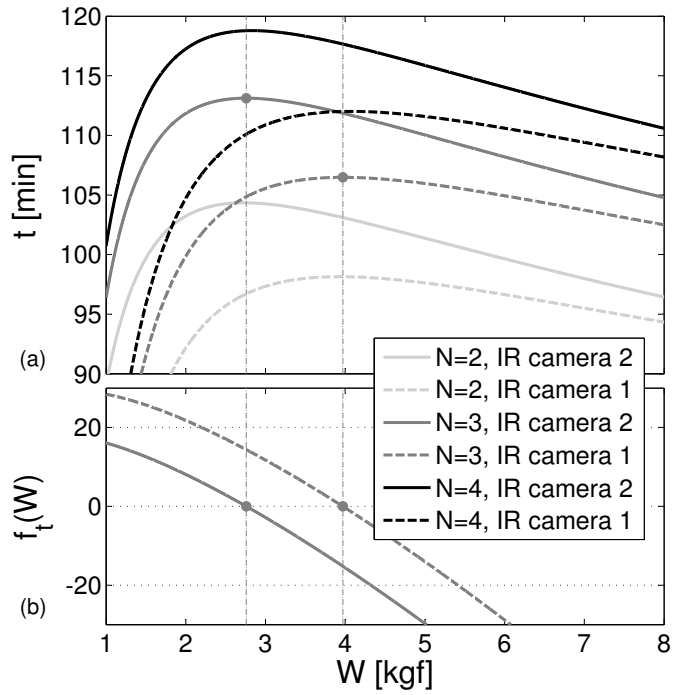

Figure 10: Endurance (a) and $f_t(W)$ function (b) for different battery/payload configurations ($b = b_{be} = 1/\sqrt[4]{3}$).

whole cruise and, beyond the maximum, this growth is not compensated by the increase in available energy (thus decreasing aircraft endurance). Weight and power required by the payload significantly affect the weight of the optimal-size aircraft by approximately 30% for the considered cameras, whereas the optimal endurance is less influenced by changes in payload characteristics, with an approximate endurance increase of 6% for the lighter camera. Conversely, the

Table 5: Endurance for different battery/payload configurations ($b = b_{be} = 1/\sqrt[4]{3}$).

battery parameters	Camera 1			Camera 2		
	W_{be} [kgf]	C_{0be} [Ah]	t_{be} [min]	W_{be} [kgf]	C_{0be} [Ah]	t_{be} [min]
$N = 2$ ($\delta = 8.336, \epsilon = -1.038$)	3.932	30.53	98.1	2.731	20.68	104.3
$N = 3$ ($\delta = 13.28, \epsilon = -1.036$)	3.970	20.59	106.5	2.759	13.96	113.1
$N = 4$ ($\delta = 18.09, \epsilon = -1.032$)	4.068	15.90	112.0	2.829	10.79	118.8

number of cells N marginally affects the optimal weight, where variations as small as -1% and $+2.5\%$ are expected when changing the battery from a 3 cell to a 2 or a 4 cell pack, respectively. In this case, the corresponding variation of maximum endurance is more significant, but still limited to -8% when changing the battery pack from $N = 3$ to 2, and $+5\%$ when changing N from 3 to 4. In this latter respect, one should also consider that the number of cells needs to be increased with aircraft weight, provided that a heavier aircraft requires a more powerful engine, usually working at a higher voltage. This means that, even if the results obtained from Eq. (37) for sizing the aircraft are plotted over a wide range of aircraft weight, a number of cells consistent with engine power needs to be selected in practical applications of the sizing process.

It is interesting to investigate, for a given battery configuration, how technological innovation in terms of payload weight and power absorption drives the sizing phase of new vehicles or influences the performance of existing platforms. Consider the aircraft configuration reported in Table 5 where $N = 3$ and Camera 1 is considered. In such a case, maximum endurance is $t_{max} = 106.5$ min and the aircraft is characterized by $W = W_p + W_{eo} + W_b = 0.186 + 2.006 + 1.779 = 3.970$ kgf and $C_0 = 20.59$ Ah. Assume that Camera 1 is replaced with Camera 2. Three scenarios can be envisaged:

1. The new payload is mounted on the existing platform, such that $W = W_p + W_{eo} + W_b = 0.114 + 2.006 + 1.779 = 3.970$ kgf, and the decrease in aircraft weight by $\Delta W = 0.114 - 0.186 = -0.072$ kgf allows increased endurance, namely $t = 110.6$ min.
2. The aircraft weight is maintained and the decrease in payload weight is balanced by an equivalent increase in battery weight and capacity respectively given by $|\Delta W| = 0.072$ kgf and $\Delta C_0 = 0.83$ Ah. In such a case, it results $W = W_p + W_{eo} + W_b = 0.114 + 2.006 + 1.851 = 3.970$ kgf, $C_0 = 20.59 + 0.83 = 21.43$ Ah, and the endurance is 111.8 min.

3. A new aircraft is sized according to the weight and power absorption of Camera 2, leading to the configuration reported in Table 5, where $N = 3$ and Camera 2 is considered. It is noted that, in this third case, the values of both aircraft weight and required battery capacity are smaller than the corresponding suboptimal values obtained in Cases 1 and 2. Also, a higher value of endurance is obtained, as reported in the second line of Table 5, related to Camera 2.

In Fig. 11 flight range as given by Eq. (41) is reported as a function of the aircraft weight for the same battery/payload configurations introduced above. The best range configuration parameters are summarized in Table 6. When

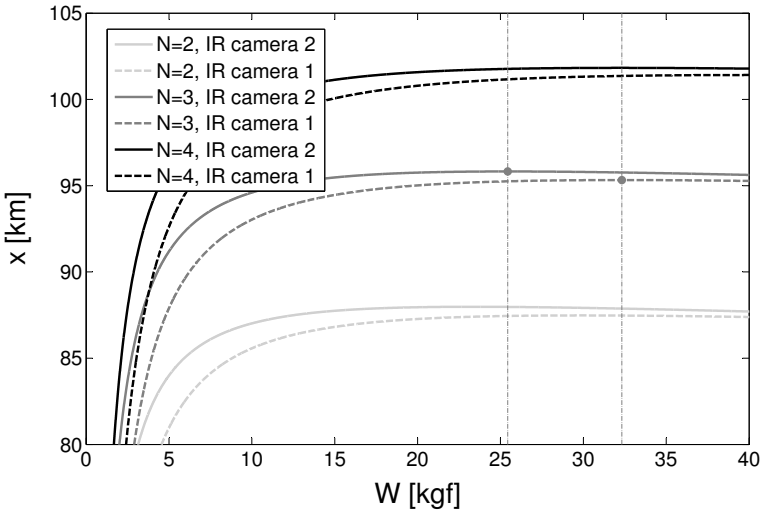

Figure 11: Range for different battery/payload configurations ($b = b_{br}(W)$).

Table 6: Range for different battery/payload configurations ($b = b_{br}(W)$).

battery parameters	Camera 1			Camera 2		
	W_{br} [kgf]	C_{0br} [Ah]	x_{br} [km]	W_{br} [kgf]	C_{0br} [Ah]	x_{br} [km]
$N = 2$ ($\delta = 8.336, \epsilon = -1.038$)	29.852	296.37	87.48	23.323	228.29	87.98
$N = 3$ ($\delta = 13.28, \epsilon = -1.036$)	32.326	215.25	95.32	25.437	167.09	95.82
$N = 4$ ($\delta = 18.09, \epsilon = -1.032$)	40.139	203.63	101.41	32.214	161.46	101.83

range becomes the performance objective of the sizing process, an optimum is obtained for large values of the total weight. Note that for all the considered configurations (Camera 1 and 2, $N = 2$, 3, and 4), the maximum is "flat",

meaning that very large variations of aircraft weight are necessary for marginal gains in terms of expected range. From the practical standpoint, this growth in aircraft weight for the "optimal" design is clearly not justified, when one considers that a heavier aircraft is more expensive and requires a more powerful engine.

In the attempt of identifying a good compromise for the optimal aircraft weight, Fig. 12 provides the Pareto front of the optimal designs in the t_{be} vs x_{br} plane, where both endurance and range performance indexes are scaled with respect to their optimal values, as a function of aircraft total weight (reported on the dots distributed along the curve). The case considered is $N = 3$ for Camera 2. The plot is limited to the non-dominated solutions, obtained for weights ranging between $W_{be} = 2.759$ kgf for the maximum endurance design, and $W_{br} = 25.437$ kgf for the design which maximizes range. Given the scale of

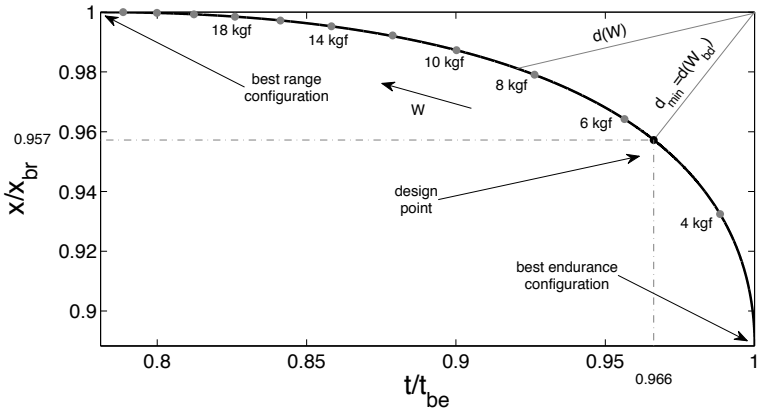

Figure 12: Pareto chart analysis (N=3, Camera 2).

the axes, each point on the plot represents the fraction of the optimal performance, where an ideal best would be represented by the point (1,1), where both maximum endurance and range are simultaneously achieved. As a consequence, the best design (indicated by the subscript *bd*) is determined numerically by selecting the point on the plot that minimizes the distance from the ideal point (1,1). For $N = 3$ and Camera 2 the weight of the best design is equal to $W_{bd} = 5.397$ kgf, with a battery pack weight equal to 2.630 kgf, a reduction of endurance and range performance equal to only 3% and 4%, respectively, with respect to the maxima in the single objective optimization problems, and a weight reduction as large as a factor approximately equal to 5 with respect to the design for maximum range only.

6. Conclusions

A model for predicting battery discharge time during a constant-power discharge process was developed and discussed. The model is based on a campaign of experiments performed with the aim of describing the behavior of lithium-polymer batteries under different operating conditions and battery pack configurations, including power request and nominal voltage of the battery.

This modeling approach allowed to estimate cruise performance of an elec trically-driven propeller aircraft. The best endurance and best range conditions were derived in terms of cruise airspeed and compared to the results available in literature, based on constant-current discharge models. A sizing process is also proposed, which allows one to size an aircraft aiming at maximum endurance or maximum range, thus providing an insight into the battery weight estimation in the framework of aircraft preliminary sizing.

The methodology was applied to a small-size electrically driven unmanned aircraft. The results show that the sizing procedure provides reasonable design in terms of battery-pack weight with respect to total aircraft weight only if maximum endurance is the design goal. Conversely, when maximum range is pursued, the best design for the same payload is characterized by a higher weight, with a modest range increment. A compromise between the two optimal designs was thus identified on the plane of the two competing objective functions.

References

[1] Harwey, S., Lucieer, A., "Assessing the Accuracy of Georeferenced Point Clouds Produced via Multi-View Stereopsis from Unmanned Aerial Vehicle (UAV) Imagery," *Journal of Remote Sensing*, 4(6), 2012, pp. 1573-1599.
doi: 10.3390/rs4061573

[2] Casbeer, D.W., Beard, R.W., McLain, T.W., Sai-Ming Li, Mehra, R.K., "Forest Fire Monitoring with Multiple Small UAVs," Proc. of the 2005 IEEE American Control Conference, 8-10 June 2005, IEEE Publ., Vol. 5, pp. 3530-3535.
doi: 10.1109/ACC.2005.1470520

[3] Rudol, P., Doherty, P., "Human Body Detection and Geolocalization for UAV Search and Rescue Missions Using Color and Thermal Imagery," Proc. of the 2008 IEEE Aerospace Conference, 1-8 March 2008, IEEE Publ., pp. 1-8.
doi: 10.1109/AERO.2008.4526559

[4] Anderson, J.D., *Aircraft Performance and Design*, 1st edition, McGraw-Hill Higher Education, New York, 1999, pp. 293-316.
isbn-13: 978-0070019713

[5] Retana, E.R., Rodrigue-Cortes, H., "Basic Small Fixed Wing Aircraft Sizing Optimizing Endurance," Proc. of the 4th International Conference on Electrical and Electronics Engineering, 5-7 Sept. 2007, IEEE Publ., pp. 322-325.
doi: 10.1109/ICEEE.2007.4345033

[6] Lawrence, D.A., Mohseni, K., "Efficiency Analysis for Long-Duration Electric MAVs," Proc. of the 2005 Infotech@Aerospace, AIAA 2005-7090, 26-29 Sept. 2005, pp. 1-7.
doi: 10.2514/6.2005-7090

[7] Peukert, W., "Über die Abhängigkeit der Kapazität von der Entladestromstärke bei Bleiakkumulatoren," *Elektrotechnische Zeitschrift*, Vol. 20, 1897, pp. 20-21.

[8] Doerffel, D., Sharkh, S.A., "A Critical Review of Using the Peukert Equation for Determining the Remaining Capacity of Lead-Acid and Lithium-Ion Batteries," *Journal of Power Sources*, Vol. 155, Issue 2, 2006, pp. 395-400.
doi: 10.1016/j.jpowsour.2005.04.030

[9] Traub, L.W., "Range and Endurance Estimates for Battery-Powered Aircraft," *Journal of Aircraft*, Vol. 48, No. 2, 2011, pp. 703-707.
doi: 10.2514/1.C031027

[10] Traub, L.W., "Validation of Endurance Estimates for Battery Powered UAVs," *Aeronautical Journal*, Vol. 117, No. 1197, 2013, pp. 1155-1166.

[11] Avanzini, G., Giulietti, F., "Maximum Range for Battery-Powered Aircraft," *Journal of Aircraft*, Vol. 50, No. 1, 2013, pp. 304-307.
doi: 10.2514/1.C031748

[12] Shepherd, C.M., "Design of Primary and Secondary Cells. An Equation Describing Battery Discharge," *Journal of The Electrochemical Society*, Vol. 112, No. 7, 1965, pp. 657-664.
doi: 10.1149/1.2423659

[13] Tremblay, O., and Dessaint, L.A., "Experimental Validation of a Battery Dynamic Model for EV Applications," *World Electric Vehicle Journal*, Vol. 3, 2009, pp. 1-10.
issn: 2032.6653

[14] Fuller, M.E., "A Battery Model for Constant-Power Discharge Including Rate Effects," *Energy Conversion and Management*, Vol. 88, 2014, pp. .199-205.
doi: 10.1016/j.enconman.2014.08.015

[15] Gatti, M., Giulietti, F., Turci, M., "Maximum Endurance for Battery-Powered Rotary-Wing Aircraft," *Aerospace Science and Technology*, Vol.

45, 2015, pp. 174-179.
doi: 10.1016/j.ast.2015.05.009

[16] Chang, T., Yu, H., "Improving Electric Powered UAVs Endurance by Incorporating Battery Dumping Concept," *Procedia Engineering*, Vol. 99, 2015, pp. 168-179.
doi: 10.1016/j.proeng.2014.12.522

[17] Moore, M.D., Fredericks, B., "Misconceptions of Electric Aircraft and their Emerging Aviation Markets," Proc. of the 52nd Aerospace Sciences Meeting, AIAA SciTech, 13-17 Jan. 2014, pp. 1-17.
doi: 10.2514/6.2014-0535

[18] Jackson, P.A., *Jane's All the World's Aircraft: development & production: 2014-15*, IHS Global, p. 335.

[19] Schweiger, H.G., Obeidi, O., Komesker, O., Raschke, A., Schiemann, M.,Zehner, C., Gehnen, M., Keller, M., Birke, P., "Comparison of Several Methods for Determining the Internal Resistance of Lithium Ion Cells," *Sensors*, Vol. 10, No. 6, pp. 5604-5625.
doi: 10.3390/s100605604

[20] Linden, D., Reddy, T.B., *Handbook of Batteries*, 3rd edition, McGraw-Hill Handbooks, New York, 2002, pp. 13-16 and 64-66.

[21] Dhameja, S., *Electric Vehicle Battery System*, 1st edition, Newnes, Oxford, Oct. 2001, pp. 44-46.

[22] Rees, E.L., "Graphical Discussion of the Roots of a Quartic Equation," *The American Mathematical Monthly*, Vol. 29, No. 2, pp. 51-55.
doi: 10.2307/2972804

[23] Raymer, D.P., *Aircraft Design: A Conceptual Approach*, 2nd edition, AIAA Education Series, Washington, DC, 1992, pp. 11-14.

[24] Veerman, H.B.C., *Preliminary multi-mission UAS design*, M.Sc. Thesis, Delft University of Technology, Aug. 2012, pp. 67-68 and pp. 221-223, available online at http://repository.tudelft.nl.

[25] Valavanis, K.P., *Advances in Unmanned Aerial Vehicles*, Intelligent Systems, Control and Automation: Science and Engineering (Book 33), Springer, 2007, pp. 387-388.

[26] Atkinson, K.E., *An introduction to numerical analysis*, 2nd edition, John Wiley & Sons, Hoboken, NJ, Apr. 1989, pp. 58-65.

[27] Brent, R.P., *Algorithms for Minimization Without Derivatives*, 1st edition, Prentice-Hall, Upper Saddle River, NJ, Mar. 2013, Ch. 5.

[28] Press, W.H., Teukolsky, S.A., Vetterling, W.T., Flannery, B.P., *Numerical Recipes: The Art of Scientific Computing*, 3rd edition, Cambridge University Press, Cambridge, UK, Sept. 2007, Ch. 10.

[29] Ostler, J.N., *Flight Testing Small Electric Powered Unmanned Aerial Vehicles*, M.S. Thesis, Brigham Young Univ., Salt Lake City, UT, Apr. 2006, pp. 1-38.

[30] Kostrzewa, J., Meyer, W.H., Laband, S., Terre, W.A., Petrovich, P., Swanson, K., Sundra, C., Sener, W., Wilmott, J., "Infrared microsensor payload for miniature unmanned aerial vehicles," Proc. of the SPIE 5090, Unattended Ground Sensor Technologies and Applications V, Vol. 5090, 18 Sept. 2003, pp. 1-10.
doi: 10.1117/12.500712